Friction **11**(6): 1079–1093 (2023)
https://doi.org/10.1007/s40544-022-0654-1
ISSN 2223-7690
CN 10-1237/TH
RESEARCH ARTICLE

Tribological mechanisms of slurry abrasive wear

Yulong LI[1,2], **Paul SCHREIBER**[1,2], **Johannes SCHNEIDER**[1,2], **Christian GREINER**[1,2,*]

[1] *Institute for Applied Material (IAM), Karlsruhe Institute of Technology (KIT), Karlsruhe 76131, Germany*

[2] *KIT IAM-ZM MicroTribology Center (μTC), Karlsruhe 76131, Germany*

Received: 21 October 2021 / Revised: 08 February 2022 / Accepted: 23 May 2022

Abstract: Abrasive wear mechanisms—including two-body and three-body abrasion—dominate the performance and lifespan of tribological systems in many engineering fields, even of those operating in lubricated conditions. Bearing steel (100Cr6) pins and discs in a flat-on-flat contact were utilized in experiments together with 5 and 13 μm Al_2O_3-based slurries as interfacial media to shed light on the acting mechanisms. The results indicate that a speed-induced hydrodynamic effect occurred and significantly altered the systems' frictional behavior in tests that were performed using the 5 μm slurry. Further experiments revealed that a speed-dependent hydrodynamic effect can lead to a 14% increase in film thickness and a decrease in friction of around 2/3, accompanied by a transition from two-body abrasion to three-body abrasion and a change in wear mechanism from microcutting and microploughing to fatigue wear. Surprisingly, no correlation could be found between the total amount of wear and the operating state of the system during the experiment; however, the wear distribution over pin and disc was observed to change significantly. This paper studies the influence of the hydrodynamic effect on the tribological mechanism of lubricated abrasive wear and also highlights the importance to not only consider a tribological systems' global amount of wear.

Keywords: abrasive wear; two-body abrasion; three-body abrasion; hydrodynamic effect; steel

1 Introduction

When hard particles are forced to move along a solid surface, abrasive wear occurs. This effect is of significance in harsh environments, such as construction and mining industries, where machinery is directly exposed to severe tribological conditions. Several studies affirm the substantial impact of abrasive wear, generating 50% of all wear problems in industries with dusty environments [1–3]. Although most machines are designed to perform in the presence of a lubricant to ensure a steady tribological performance, particles being trapped between interacting surfaces are inevitable. This can cause abrasive wear in lubricated contacts and lead to tribological failure, corroborating the need for fundamental and applied research in the field of abrasive wear.

To accurately describe the acting mechanism during abrasive wear processes, researchers classified it into two-body abrasion and three-body abrasion [4–7]. Two-body abrasion denotes wear by "stuck" particle sliding against the surface of a counter body. During sliding, the particles can cut and plough the counter body's surface. Three-body abrasion means that wear is generated by free rolling particles between interacting surfaces. Commonly it is assumed that the wear rates caused by two-body abrasion are higher than those caused by three-body abrasion because particles are continually cutting and ploughing during two-body abrasion, while particles are assumed to be rolling most of the time during three-body abrasion. With different experimental conditions and materials, abrasive particles can generate wear through cutting, ploughing, fatigue, and cracking [3, 8, 9].

* Corresponding author: Christian GREINER, E-mail: christian.greiner@kit.edu

Misra and Finnie [7, 10–12] studied the tribological performance of two-body and three-body abrasion under dry conditions. In their research, two-body abrasion was found to be about nine to twelve times as effective in removing material as three-body abrasion. Williams and Hyncica [13, 14] revealed the mechanism of abrasive wear in lubricated contacts using a model based on the particle dimension d and film thickness h. Beyond a critical ratio d/h, the wear mechanism was reported to change from three-body abrasion to two-body abrasion, and wear increased with d/h. Wear mechanism and wear performance were also found to be linked to further parameters, such as abrasive size [15, 16], abrasive type [17], abrasive concentration [18, 19], or load [20, 21]. Most of the results and theories indicate that the wear rates caused by two-body abrasion are much higher than those for three-body abrasion.

Considering the above, efforts have been made to enhance the abrasive wear performance of tribological systems. Xiao et al. [22] investigated the effects of two additives (polystyrene and silicon nitride) on the tribological performance of water-based slurries with silicon dioxide or alumina abrasives. Polystyrene reduced wear but increased friction, while silicon nitride showed a positive effect on both abrasion resistance and friction reduction. Da Silva et al. [23] studied micro-textured tools in machining and micro-abrasion tests. Texturing increased the tool life in the machining tests, but resulted in a pronounced increase in the coating wear rates in the micro-abrasion experiments. In addition to these attempts, coatings [24] and novel materials [25] were also investigated as strategies for friction and wear reduction in abrasive wear. However, only limited research [26, 27] associates lubricated abrasive wear with hydrodynamic effects along the Stribeck curve [28], causing a lack of experimental support on the Stribeck curve's applicability for lubricated abrasive wear. The Stribeck curve visualizes how friction in a system may change due to a hydrodynamically induced fluid film that can separate contacting asperities and partially carry the applied normal load, which is a conventional approach to suppress wear under normal lubrication [26, 29–32]. However, to the best of our knowledge, how an increasing fluid film thickness influences lubricated abrasive wear remains unclear.

This work aims to investigate the influence of sliding speed on lubricated abrasive wear utilizing both multi-step and constant speed tests. In the multi-step speed experiments, the influence of the abrasive size on the hydrodynamic effect was studied using two kinds of slurries with different particle sizes (5 and 13 μm). The presence of a speed-induced hydrodynamic effect was only observed when using the 5 μm slurry as interfacial media. The 5 μm slurry and two speeds were then chosen to study how the hydrodynamic effect influences abrasive wear, including friction and wear of both pin and disc. Furthermore, a brief explanation of the wear results is given based on the wear mechanism.

2 Experimental

2.1 Materials

The tribological experiments were carried out using a pin-on-disc configuration with pins and discs made from bearing steel (100Cr6, AISI 5210). The bearing steel discs, having a diameter of 70 mm, were purchased from Eisen Schmitt (Karlsruhe, Germany). They underwent a hardening and tempering process to reach a hardness of nominally 800 HV. All the discs were fine-ground on a cup grinding machine (G&N MPS 2 R300, Erlangen, Germany) with corundum grinding wheels of grit EK200, resulting in mean roughness values ranging from Ra = 0.08 to 0.12 μm (measured by the tactile surface profilometer; T8000 R120-400, HOMMEL-ETAMIC, Villingen-Schwenningen, Germany). The radial flatness along the frictional track was below 1 μm (measured by the FRT MicroProf optical surface profilometer; MPR 1024, Bergisch Gladbach, Germany). The pins were purchased in the form of 8 mm diameter spheres and then flatted to a circular area of 7.33 mm in diameter by grinding and polishing. They were purchased from KGM (Fulda, Germany) and employed in an as-received condition with a hardness of 700 HV. The flattened surfaces had roughness values ranging from Ra = 0.02 to 0.04 μm and a flatness below 0.6 μm. All pins and discs were demagnetized and cleaned with isopropanol for

15 min in a sonicating process before the tribological experiments.

Two kinds of water-based aluminum oxide abrasive slurries with different particle sizes (5 and 13 μm, according to the FEPA grain standards) were purchased from Joke (Lapping medium BIOLAM®, Bergisch Gladbach, Germany) with a nominal concentration of 12.5 wt%. The size distribution of the particles in the slurries was measured by the laser granulometer (CILAS 1064, Orléans, France), presented in Fig. 1(a). Both slurries show a narrow and slightly bimodal particle size distribution. The scanning electron microscopy (SEM) image of a dried slurry shown in Fig. 1(b) confirms that no specific shape exists. The results for dynamic viscosity measurements are presented in Supplementary Note 1 in the Electronic Supplementary Material (ESM).

2.2 Tribological testing

Tribological tests were carried out on a pin-on-disc tribometer (Fig. 2) built by Swiss Center for Electronics and Microtechnology, Inc. (Neuchatel, Switzerland). During the experiments, the pin was mounted on a self-aligning pin holder to ensure proper flat-on-flat contact, and a normal force of 2 N was applied to the pin by dead weights. To limit the influence of a velocity gradient due to the large contact area [33], a mean sliding radius of 21 mm was selected. For each test, 100 ml slurry was added to the experimental setup before the experiment to ensure a bath-like condition around the contacting surfaces throughout the test. The friction force was determined by measuring the deflection of an elastic arm.

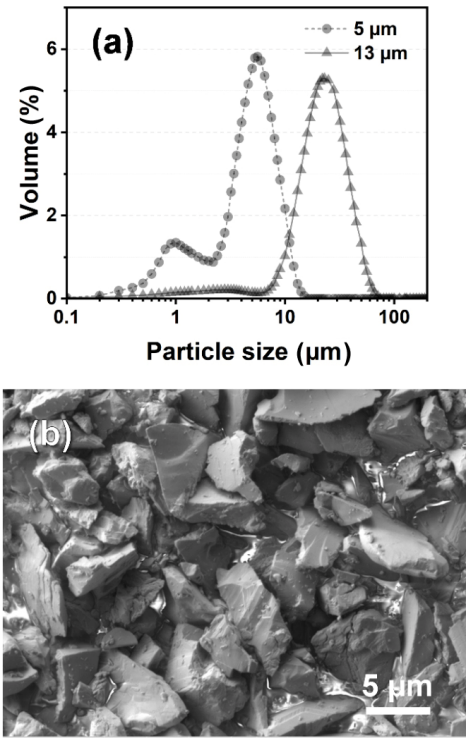

Fig. 1 Characterization of the particles in the slurry: (a) particle size distribution; (b) SEM image of alumina particles in the 5 μm slurry.

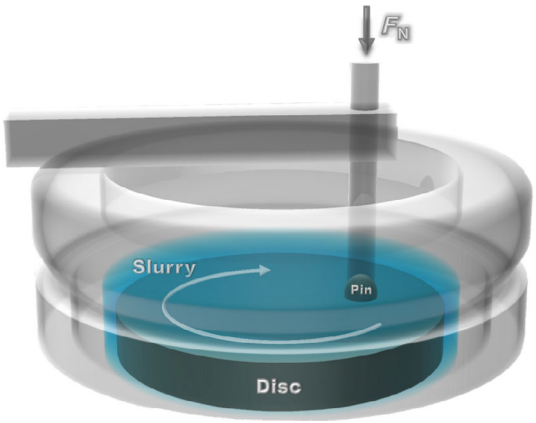

Fig. 2 Experimental set-up of the pin-on-disc tribometer.

Two kinds of speed sets were utilized: multi-step and constant speeds. For the multi-step speed experiments with the 5 and 13 μm slurries, the sliding speed was decreased stepwise from the fastest (400 mm/s) to the slowest (50 mm/s) speed (the change in speed is visualized in Fig. 3), holding each of the nine steps for 2 min in order to generate the data that can be evaluated as Stribeck curves. Each complete multi-step speed set (referred to as a ramp) was repeated five times, resulting in a total sliding distance of 846 m. To avoid any impact that may originate from

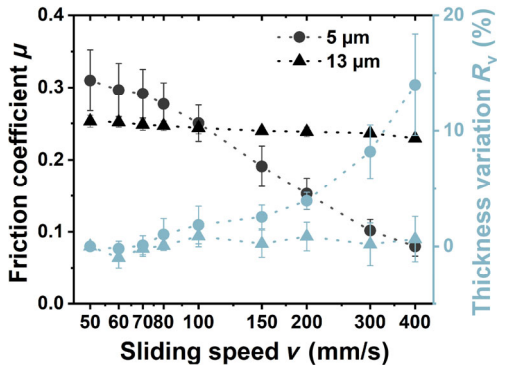

Fig. 3 Friction coefficient and relative variation in film thickness R_v of frictional surfaces as a function of sliding speed.

a potential running-in process, only the last three ramps were chosen to calculate the mean value of the friction coefficient at each sliding speed. All the experiments were carried out at least three times with completely new pins and discs.

The fastest (400 mm/s) and the slowest (50 mm/s) speeds of multi-step speed set were selected to perform constant speed tests with the 5 μm slurry to reveal the wear mechanism in different lubrication regimes. The second variable in the constant speed tests was the sliding distance, with values of 0.13 (1 revolution of the disc), 1, 10, 50, and 846 m for each speed. With the aim of evaluating the wear performance at 400 and 50 mm/s, experiments with the longest sliding distance (846 m) were repeated three times with fresh samples.

2.3 Characterization

For the multi-step speed tests, the distance between the pin and the disc was measured with a capacity sensor on the top of the pin holder. When the speed varies during the multi-step speed experiments, the change of the distance between the pin and the disc can also be monitored and interpreted as the change in the film thickness Δh. The values of Δh are also the average of three experiments. With this approach, the changes in separation between pin and disc due to wear are inevitably included. However, the change in film thickness only considers 14 seconds before and after the speed change; thus, wear-induced separation changes are negligible and as a first-order approximation ignored. The film thickness value at 50 mm/s is regarded as the reference, where the film thickness is assumed to only be determined by the particle size d of the slurry, 5 and 13 μm. With this assumption, the relative variation in film thickness R_v can be calculated (Eq. (1)):

$$R_v = \frac{\Delta h}{d} \cdot 100\% \tag{1}$$

Wear was considered for both pin and disc. The pins' wear was measured as a loss in weight with a precision scale (R160P, Sartorius research, Germany), with a resolution of 0.01 mg. The wear-induced volume loss of the discs was determined with the FRT MicroProf optical surface profilometer's data and then converted to a weight loss. Details of the volumetric wear calculating are provided in Supplementary Note 2 in the ESM.

For the microstructural characterization, the focused ion beam/scanning electron dual-beam microscope (FIB/SEM; Helios NanoLab Dual-beam 650, FEI, USA) was used. The worn surfaces of both pin and disc were observed by the SEM. Cross-sectional SEM images were taken perpendicularly to the sliding direction to study the effect of abrasive wear on the subsurface material. Two platinum layers were deposited before ion milling to limit the damage due to the ion beam, the first one deposited with the electron beam and the second by the ion beam.

3 Results

3.1 Multi-step speed experiments

The results of the multi-step experiments are presented in Fig. 3, giving an overview of the friction coefficients under abrasive wear as well as the relative variation in film thickness R_v between the two frictional surfaces as a function of the sliding speed. As the speed increases, the friction coefficient decreases from 0.31 at 50 mm/s to 0.08 at 400 mm/s—a drop in friction of about 2/3. Simultaneously, a significant variation in film thickness can be observed for the 5 μm slurry with sliding speed; the film thickness increases 14% at 400 mm/s under abrasive wear. The results for the 13 μm slurry exhibit a different trend compared to the 5 μm one, and the sliding speed has a negligible effect on the friction coefficient. The friction coefficient only drops from 0.25 to 0.23 when the sliding speed increases from 50 to 400 mm/s. Simultaneously, the increase in film thickness is negligible and about 1%.

3.2 Constant speed experiments with 5 μm slurry

In Fig. 4, the friction coefficient and wear loss for the experiments with the 5 μm slurry at two constant speeds are shown. For a sliding speed of 400 mm/s, the friction coefficient almost doubled, from 0.06 at the beginning of the experiment to approximately 0.12 in the later stages. For a low speed of 50 mm/s, the friction coefficient rises from 0.15 at the beginning of the test to around 0.25 at the end. If we compare

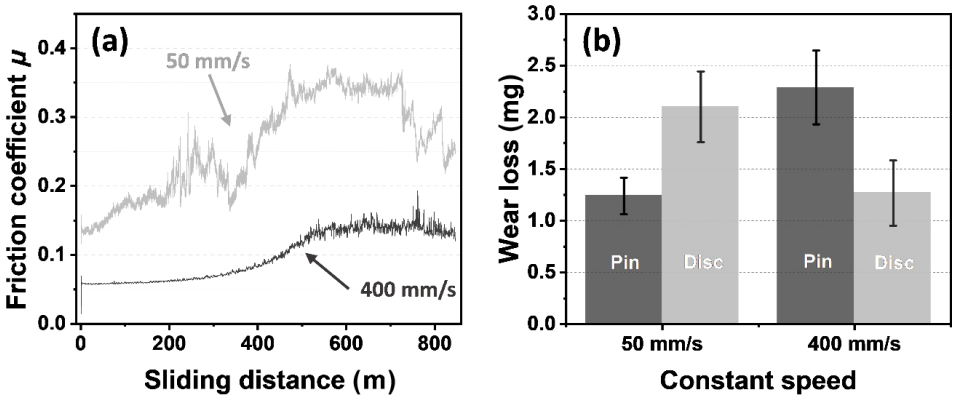

Fig. 4 Results for the 5 μm slurry at constant sliding speeds of 50 and 400 mm/s for a maximum sliding distance of 846 m: (a) friction coefficient as a function of sliding distance; (b) wear results of pin and disc for the two constant speeds.

the overall average friction coefficients for the constant speed experiments, the ratio between the value for the tests at 400 mm/s to the one at 50 mm/s—μ_{400}/μ_{50}—is approximately 1/3. Another marked contrast is the deviation of the friction coefficient, which was much more prominent throughout the whole constant speed tests at the low speed (50 mm/s).

The data in Fig. 4(b) show the results of the wear analysis of both frictional surfaces after experiments at different constant speeds. The sum of the wear of the entire tribological system after high speed (400 mm/s) and low speed (50 mm/s) experiments are 3.54±0.67 and 3.34±0.52 mg, respectively. Although the total amount of wear remains almost the same for the two different constant speeds, the wear loss has a different distribution between pin and disc. At the low-speed (50 mm/s) tests, the wear produced on the pin is only about 1.24±0.18 mg, whereas the disc has significantly more wear, resulting in a weight loss of 2.1±0.34 mg, which is 1.7 times that of the pin. The wear distribution is inverted for the high-speed (400 mm/s) tests, leading to a wear loss of 2.29±0.36 mg for the pin and 1.27±0.32 mg for the disc.

Figure 5 presents the SEM images of pin surfaces after different sliding distances at constant speeds for the sliding distances of 10, 50, and 846 m. All worn surfaces were imaged in the center of each pin. After 10 m of sliding at 50 mm/s, clear and dense grooves are visible on the worn surface of the pin in Fig. 5(a), and the width and depth of grooves do not differ

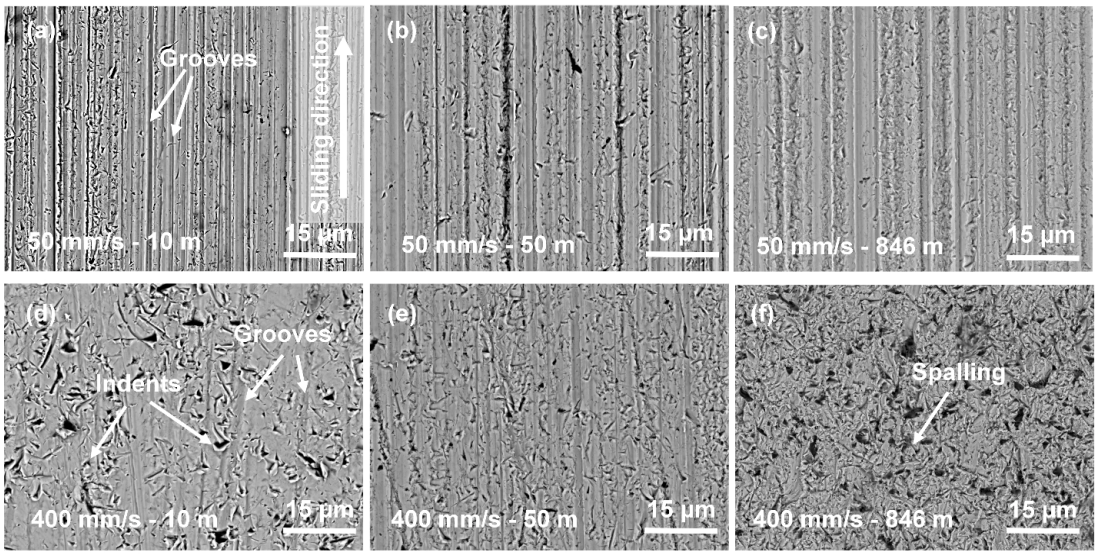

Fig. 5 SEM images of pins after constant speed experiments: (a) sliding 10 m at 50 mm/s; (b) sliding 50 m at 50 mm/s; (c) sliding 846 m at 50 mm/s; (d) sliding 10 m at 400 mm/s; (e) sliding 50 m at 400 mm/s; and (f) sliding 846 m at 400 mm/s.

considerably. As the sliding distance increases to 50 m at 50 mm/s (in Fig. 5(b)), the worn surface of the pin does not change much compared with that after 10 m, with plenty of grooves and few indents. With the sliding distance increasing to 846 m, where the material had suffered severe damage, wider grooves and more indents can be seen in Fig. 5(c) compared to the surfaces after 10 and 50 m. The worn surfaces of the pins after high-speed (400 mm/s) experiments show different features from low-speed (50 mm/s) ones. In Fig. 5(d), which shows the worn surface after 10 m at 400 mm/s, only some indents and very few grooves can be seen. After 50 m at 400 mm/s (in Fig. 5(e)), indents have covered most of the wear track, and grooves are rare and shallow. With the sliding distance rising to 846 m at 400 mm/s (in Fig. 5(f)), one can observe that the wear track is entirely covered by indents. As for the short-distance experiments at 400 mm/s (10 and 50 m), sparse grooves can be distinguished with unclear traces. The difference in the worn surfaces at different constant speeds also appears on the discs (Fig. 6), which are the counter bodies for the pins presented in Fig. 5. The worn surfaces of the discs show the same trends as the pins, with more grooves after low-speed experiments (Figs. 6(a)–6(c)) and more indents after high-speed experiments (Figs. 6(d)–6(f)). Notably, the grooves in Fig. 6 are not all formed during the tribological test; those grooves perpendicular or approximately perpendicular to the sliding direction are the vestiges of the grinding process during sample preparation.

For a better understanding of the different acting mechanisms of abrasive wear, Fig. 7 shows the cross-sectional SEM images of the tribologically deformed subsurface material, which were taken in the middle of the pin; a cross-sectional image of an undeformed pin is shown in Fig. 7(e). For the unloaded pin, the surface is smooth, and no cracks can be observed in the subsurface area. The general fine-grained layer [34] results from the grinding process during sample preparation. For the pin after sliding 50 m at 50 mm/s and the one after 846 m (Figs. 7(a) and 7(b)), a geometry alteration in the vicinity of the surface can be noticed. Hardly any subsurface cracks can be found in the cross-sectional SEM images after 50 m at 50 mm/s (Fig. 7(a)). Similarly, only sporadic cracks exist in the subsurface after 846 m at 50 mm/s (Fig. 7(b)). A considerable number of subsurface cracks can be observed in the early stage of the experiments at 400 mm/s (Fig. 7(c)). For the high-speed experiments (400 mm/s) after 846 m, a network of cracks has developed into a defect rich subsurface microstructure, forming a fractured subsurface with depths from 200 to 650 nm (Fig. 7(d)).

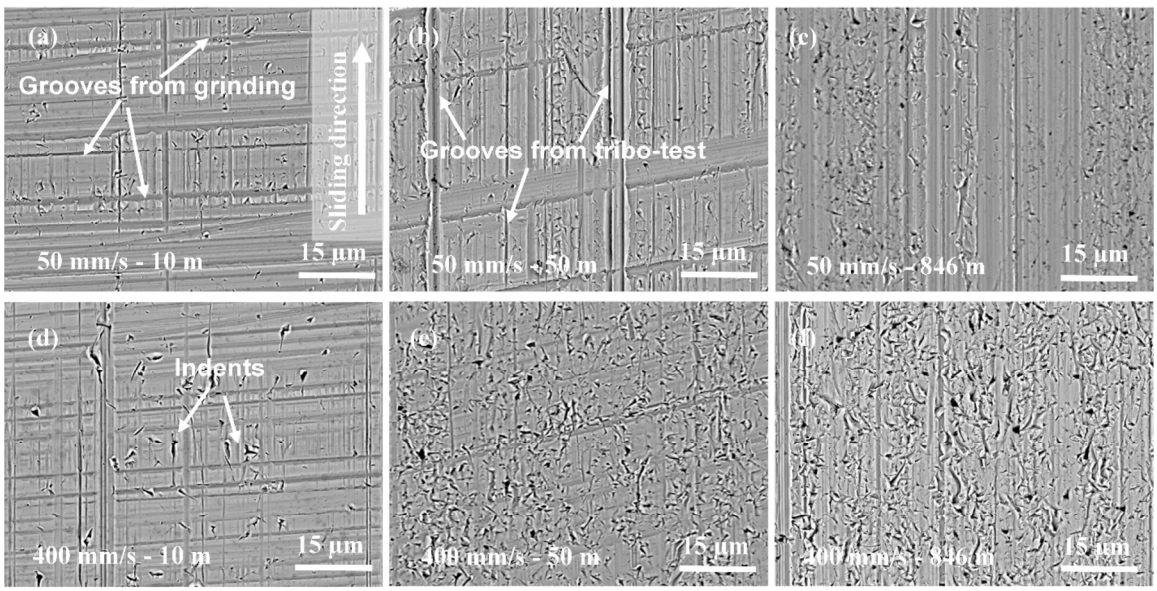

Fig. 6 SEM images of discs after constant speed experiments: (a) sliding 10 m at 50 mm/s; (b) sliding 50 m at 50 mm/s; (c) sliding 846 m at 50 mm/s; (d) sliding 10 m at 400 mm/s; (e) sliding 50 m at 400 mm/s; and (f) sliding 846 m at 400 mm/s.

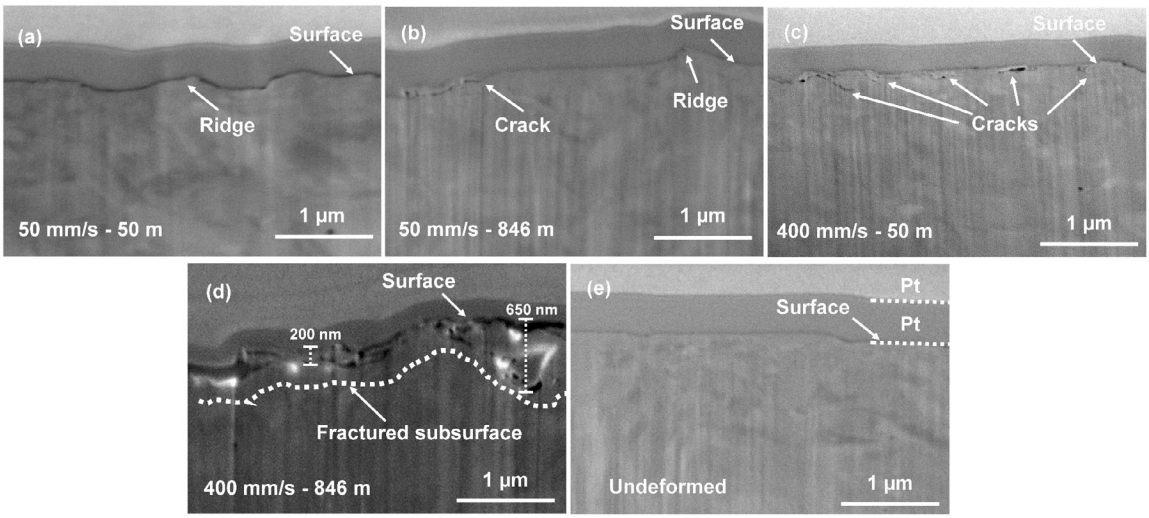

Fig. 7 Cross-sectional SEM images of pins: (a) sliding 50 m at 50 mm/s; (b) sliding 846 m at 50 mm/s; (c) sliding 50 m at 400 mm/s; (d) sliding 846 m at 400 mm/s; and (e) undeformed pin.

4 Discussion

4.1 Friction

In the multi-step experiments conducted with the 5-μm slurry as the interfacial medium, a drastic decrease in friction coefficient was observed with increasing sliding speed (Fig. 3), combined with a significant relative variation in film thickness. Such speed-induced hydrodynamic effects are common in the literature, whether the interfacial media are oil-based lubricants [35–37] or abrasive slurries [26, 27]. At low speed of up to 50 mm/s, the film thickness does not change much with increasing speed. The load is mostly carried by particles between the frictional surfaces, so the friction coefficient is only slightly decreasing with speed in this low-speed regime (50–80 mm/s). This is an indication of "boundary lubrication" at low speeds for the multi-step experiments. A sharp increase in film thickness exists at higher speeds (200–400 mm/s), and a maximum value of a 14% increase in film thickness can be measured. This points to "mixed lubrication" as it was reported before [28, 38, 39]. The increasing film thickness can help separate contact asperities and partially carry the tribological load. At this point, the load is supported by both particles and the solvent in the slurry, which leads to a significant drop in friction coefficient at high speeds (200–400 mm/s). Similar to the previous research using abrasive slurries as an interfacial medium [40, 41], pure "hydrodynamic lubrication"—a full separation of contacting surfaces resulting in very low friction coefficients—cannot be observed in our experiments.

For the multi-step experiments with the 13 μm slurry, both friction coefficient and film thickness did not change significantly with the sliding speed (Fig. 3). The initial separation between the frictional surfaces is 13 μm when working with the 13 μm slurry as interfacial medium, which is 2.6 times the separation for the 5 μm slurry. On the one hand, the large initial film thickness will make the speed-induced thickness change negligible; on the other hand, the wide gap will also make it difficult to build up enough hydrodynamic pressure to carry the tribological load. This is why the gap between the frictional surfaces remains rather constant. With the speed increasing from 50 to 400 mm/s, we observe only little change in film thickness and friction coefficient during the multi-step experiments. This demonstrates that the particle size plays an essential role under lubricated conditions; larger particles between frictional surfaces seem to hinder the generation of sufficient hydrodynamic pressure to separate the two contacting bodies.

When it comes to the constant speed experiments using the 5 μm slurry as the interfacial medium, the hydrodynamic effect at 400 mm/s lowers friction

by about 2/3 compared with the friction coefficient at 50 mm/s (Fig. 4). According to Refs. [26, 29, 30], one would expect a wear reduction for the 400 mm/s experiments compared to the 50 mm/s ones. This is however not what we observe when the wear for both pin and disc are considered (Fig. 4(b)).

4.2 Wear mechanisms

Wear analysis was performed for the samples utilized in constant speed experiments and the 5 μm slurry. As the experiments were carried out in bath conditions for the slurries, there were always sufficient particles between the frictional surfaces. The size of the particles in the slurry (5 μm) is a factor of one order of magnitude higher than the flatness (pin ≤ 0.6 μm, disc ≤ 1 μm) and roughness (pin: Ra = 0.02–0.04 μm, disc: Ra = 0.08–0.12 μm) of the frictional surfaces, which indicates that solid contact primarily was formed between particles' and samples' surfaces. In other words, there was no directly tribological contact between the pin and the disc. The indents and grooves on the worn surface (Figs. 5 and 6) likely were generated by the particles. The results of the SEM examinations show that from the beginning (10 m) to the end (846 m) of the tribological experiments, more deep grooves can be seen for the 50 mm/s experiments (Figs. 5(a)–5(c)) and Figs. 6(a)–6(c)), and more indents appear on the surfaces for the 400 mm/s experiments (Figs. 5(d)–5(f) and Figs. 6(d)–6(f)). The dependence of the wear mechanism on the sliding speeds can be clarified by using the model from Williams and Hyncica [13, 14]. This model illustrates the transition from sliding to rolling to be associated with a critical ratio of d/h, where d is the particle dimension and h is the separation of the surfaces. In their work, an increase in particle size or decrease in film thickness led to more effective attack angles, which can result in the generation of grooves on the worn surface. In contrast, a small ratio of d/h allows particles to roll or tumble between the surfaces, associated with characteristic indentations on the surfaces showing slight directionality. In our experiments, the particle size d is constant and narrowly distributed (Fig. 1), and a speed-induced hydrodynamic effect determined the film thickness h ($h = d + \Delta h$). Based on the results presented in Fig. 3, the increase in film thickness can reach values up to 14% when the sliding speed increases from 50 to 400 mm/s. The resulting gap at 400 mm/s presumably allows more particles to roll between pin and disc, while at 50 mm/s particles are more inclined to cut or groove, which leads to two very different characteristics of the worn surfaces (Figs. 8(a) and 8(b)). This line of reasoning strongly suggests a change in how the particles move through the contact from sliding to rolling as the speed increases from 50 to 400 mm/s (Figs. 8(c) and 8(d)). In addition, this can be regarded as a transition from two-body abrasion to three-body abrasion [3, 7] or from grooving abrasion to rolling abrasion [42].

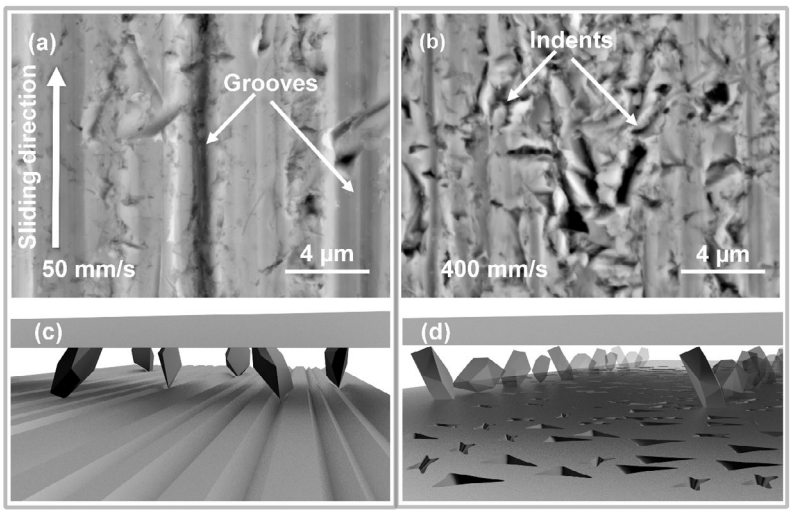

Fig. 8 Two distinct worn surfaces generated by particles in different kinematic states and their schematics: (a) heavily-grooved surface at 50 mm/s by two-body abrasion; (b) scattered indented surface at 400 mm/s by three-body abrasion; (c) schematic of two-body abrasion in the lubricated contact; and (d) schematic of three-body abrasion in the lubricated contact.

Another observation strengthens this hypothesis: In several SEM images, a periodic pattern of indents was found on the samples' surfaces after high-speed (400 mm/s) experiments. Figure 9(a) shows the SEM image of a disc's surface after 846 m of sliding at 400 mm/s. Here, two distinctly different shapes of indents alternately appear along the sliding direction. As shown in the schematic (Fig. 9(b)), e.g., one can imagine particles with large aspect ratios, or that are less sharp in a specific direction, and that would create such periodic patterns of indents. A Supplementary Video is provided in the ESM to illustrate the formation of a periodic pattern of indents. Although the typical worn surface of three-body abrasion has been widely studied [14, 43], such a trajectory of an individual rolling particle was seldom reported.

To further understand the processes behind the changes in wear mechanisms, cross-sectional investigations of the tribologically deformed subsurface layers were performed (Fig. 7). A cross-section under parallel grooves (Fig. 7(a)) shows no recognizable subsurface cracks when the sliding distance is 50 m (Fig. 7(a)). Only a few subsurface cracks can be observed even if the sliding distance is at its maximum value of 846 m (Fig. 7(b)). To some extent, particles are "stuck" in the contacting counter surface, resulting in microcutting and microploughing [14], which did not lead to subsurface cracks in our tribological model experiments. The limited amount of subsurface cracks (highlighted with an arrow in Fig. 7(b)) inside the groove might be the result of small particles that were able to roll inside the groove [44]. Perceptible ridges in Figs. 7(a) and 7(b) were formed by the displacement of material due to plastic deformation [45, 46]. Thus, the predominant wear mechanism at 50 mm/s is two-body abrasion, and material is removed from the contact by microcutting and microploughing.

In contrast to the cross-sections at 50 mm/s, a considerable amount of cracks can be observed already at the beginning of the test at 400 mm/s and for 50 m of sliding (Fig. 7(c)). As the sliding distance increases to 846 m, a very high defect density in the subsurface is observed with a depth of around 200 nm to 650 nm. When the sharp edges of the particles (Fig. 1(b)) indent the surface during the rolling process (Fig. 7(d)), each contact can be seen as an indentation. Based on earlier research [47–50], such sharp indentations can generate a localized plastic deformation zone and material displacement beneath the indentation contact. Compared with the repeated plastic deformation inside the grooves for the experiments at 50 mm/s, the surface after testing at 400 mm/s with scattered indents indicates an intersected and non-directional plastic deformation. One could expect this to result in more wear for the samples at 400 mm/s, as it has been proven that distributed plastic deformation is more destructive than a repeated plastic contact at the same location [51]. Furthermore, many particles rolling between the contact's gap might result in cyclic loading and unloading of the surface, creating a series of closely spaced indentations. A period of repeated elastic–plastic loading would certainly cause microstructural changes [52–55] together with cyclic softening or hardening, leading to crack formation and propagation in the plastic deformation zone below or at the surface, which eventually can lead to surface fatigue (Fig. 7(d)). Meanwhile, the fractured subsurface with a certain thickness (around 200 to 650 nm) seems reasonable if

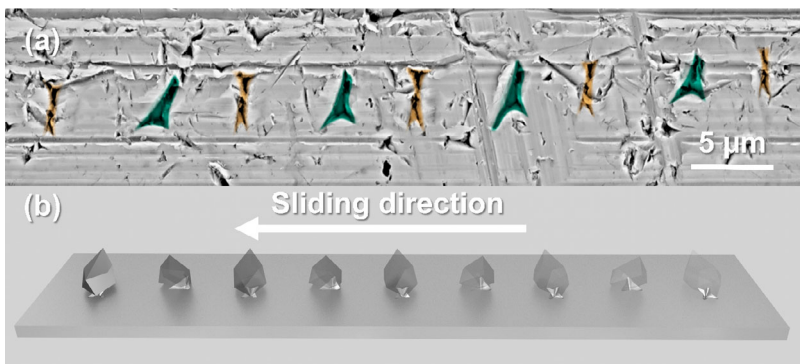

Fig. 9 Periodic pattern of indents: (a) SEM image of a disc after 50 m of sliding at 400 mm/s, and a periodic pattern of indents can be observed; (b) schematic of periodic indentation generation in (a).

one considers each indentation as a hardness test by a particle. The depth of the plastic deformation zone is then determined by the materials' hardness, the contact pressure, and the particles' geometry, which are within a small range in the experiment. The indented surface as well as the fractured subsurface is very similar to that observed by previous researchers [3, 8, 56–60], indicating the existence of surface fatigue. Since subsurface cracks occurred already at the early stages (50 m of sliding), surface fatigue could make the materials vulnerable to removal during subsequent impacts. As a consequence, with particles' kinematic changed due to a hydrodynamic effect, surface fatigue might be a determinant factor for the wear at 400 mm/s.

A reference experiment at a constant speed of 400 mm/s was performed using the 13 μm slurry, where the tribological system cannot benefit from hydrodynamic pressure because of the big particle size in the slurry (Fig. 3). In line with the so far presented hypothesis, the surface mainly shows indications of two-body abrasion caused by particle sliding (Fig. 10(a)). Only very few subsurface cracks appear after 846 m of sliding at 400 mm/s (Fig. 10(b)).

4.3 Wear

Using the terms two-body abrasion and three-body abrasion or grooving abrasion and rolling abrasion to clarify the mechanisms on abrasive wear is still under debate [61, 62]. Nevertheless, to the best of our knowledge, the majority of published research reported that three-body abrasion generates less wear compared to two-body abrasion [3, 6–8, 11, 13, 14, 43, 61, 62]. For the high-speed (400 mm/s) experiments conducted with the 5 μm slurry, there is both a change in the kinematics of how the particles move in the contact as well as an additional hydrodynamic effect. Still, our results cannot be interpreted in accordance with the previous theory above. The wear results have at least two aspects, which cannot easily be understood: First, the total amount of wear for the high-speed (400 mm/s) and low-speed (50 mm/s) experiments do not vary much; second, the wear distribution between pin and disc is inversed (Fig. 3(b)).

As stated by previous researchers, abrasion of a metal involves a certain minimum strain energy, sufficient to saturate its capacity for work hardening under tribological load [63]. This energy, for some metals at least, happens to be close to the melting energy. Therefore, the energy approach might be a very effective way to explain the wear results [64]. The dissipated energy E in the frictional surfaces is calculated as the work of the friction force F. For each sliding distance Δx, the dissipated energy ΔE can be calculated in Eqs. (2) and (3):

$$\Delta E = \int_0^{\Delta x} F \mathrm{d}x \tag{2}$$

$$P = \frac{E}{t} \tag{3}$$

The total dissipated energy E for a sliding distance of 846 m in the constant speed experiments can be calculated by Eq. (2). Then, the friction power P can be calculated from E and the testing time t as shown in Eq. (3).

The results for the dissipated energy and the frictional power for the constant speed experiments after 846 m of sliding can be seen in Table 1. Due to a hydrodynamic effect, the dissipated energy decreases from 447 J at 50 mm/s to 170 J at 400 mm/s. However,

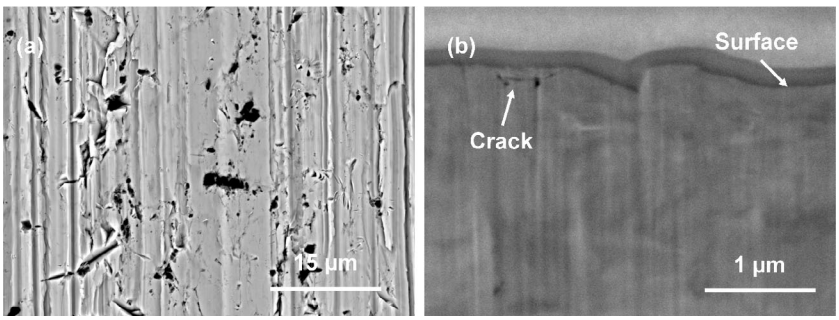

Fig. 10 Pin after testing with the 13 μm slurry at 400 mm/s: (a) SEM image of the worn surface; (b) cross-sectional SEM image of the worn surface.

Table 1 Wear results for the experiments with the 5 μm slurry and after a sliding distance of 846 m.

Speed (mm/s)	Total wear (mg)	Dissipated energy (J)	Friction power (mW)
50	3.34	447	26.4
400	3.56	170	80.6

if the experiments' run times are taken into account, the friction power at 400 mm/s is three times the one at 50 mm/s. The combination of high friction power and fatigue surface could exacerbate the wear on the frictional surfaces at 400 mm/s, causing the total amount of wear observed after sliding at 400 m/s to be almost the same as after sliding at 50 mm/s—despite the lower friction coefficient. Friction power—or the rate of energy dissipation—appears to play a key role in the generation of abrasive wear during the experiments.

Another question that remains is why at 400 mm/s the wear of the pin increases, and the wear of the disc decreases compared to experiments at 50 mm/s. As discussed above, surface fatigue generated by indentations is an essential factor for the wear performance during the experiments at higher speeds. Possibly the contact area A could play an essential role since different indent densities would induce variable levels of subsurface deformation. Thus, the dissipated power density ρ could be an important parameter when it comes to finding a possible explanation for the different reactions of pin and disc to a speed-induced change of wear mechanism; it has previously already been used to compare friction pairs with different contact areas [65]. The dissipated power density ρ is defined as the ratio between the friction power and the contact area A:

$$\rho = \frac{P}{A} \tag{4}$$

For our pin-on-disc experiments, the pin's contact area is in permanent contact, while any given point on the disc is only in intermittent contact. The disc's contact area is almost 23 times that of the pin, which means that the dissipated power density for the pin is as well higher than that for the disc. When—as assumed—surface fatigue dominates the wear generation at 400 mm/s, a high dissipated power density will most likely result in more severe wear conditions for the pin when compared to the experiments run at 50 mm/s—resulting in a higher material loss due to fatigue. Contrarily to this effect, the disc's wear decreases at 400 mm/s compared to 50 mm/s as the dissipated power density may not be high enough to cause a completely fatigued surface on the disc.

This line of thinking can not only be supported by the evidence that a more severe fatigued surface can be observed in Fig. 5(f) than that in Fig. 6(f), but also by a cross-sectional SEM image of the disc after 846 m at 400 mm/s (Fig. 11), where fewer cracks can be observed compared with that of the pin (Fig. 7).

Owing to the complexity of tribology—especially in abrasion—not one single mechanism can explain all the observations in an experimental study. There are two antithetical hypotheses in the literature on the correlation between speed and abrasive wear rate. Bose and Wood [66] reported a positive correlation between speed and abrasive wear rate, which they attributed to the more severe hydrodynamic interaction between the slurry and the test specimen at higher speeds. In our results, the increased wear on the pin with speed was also contributed by hydrodynamic interaction. In contrast, an opposite trend was observed by Gee et al. [19], where the wear volume was largely independent of sliding speed but increased somewhat for very low speeds. The hydrodynamic film in abrasive wear (Fig. 3) may help support Gee's point of view on the free ball machine; the film thickness increases with speed, which may result in the tendency of the ball to slip on the shaft, and then finally lead to an apparent decrease in wear.

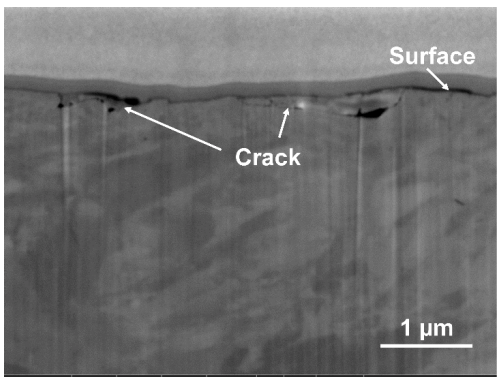

Fig. 11 Cross-sectional SEM image of disc after testing for 846 m at 400 mm/s.

Interestingly, if the wear of the pin and disc are both considered, as we did in this paper (Fig. 4(b)), these two conflicting results can show up in one set of experiments. We throw light on a dark corner of the wear mechanism under lubricated abrasive wear, illustrating that three-body abrasion can cause more wear than two-body abrasion, and also highlight the importance of taking care of the wear from both contact sides. Many important parts of this puzzle are still worth investigating. For example, will particle size effects be different from previous reports [9, 16, 67] because of a change in wear mechanism? How do the friction power and the friction power density influence wear when using a slurry with a bigger particle size?

5 Conclusions

In this contribution, we investigated the tribological mechanisms of abrasive wear in lubricated tribological model systems. Bearing steel (100Cr6) was chosen for both pin and disc to form a flat-on-flat contact, with 5 and 13 μm slurries as interfacial media. Two kinds of speed experiments were performed for different purposes: multi-step speed experiments with sliding speeds between 50 and 400 mm/s aimed at studying the influence of abrasive particle sizes on the hydrodynamic effect. The 5 μm slurry and two constant sliding speeds were chosen to study how the hydrodynamic effect influences abrasive wear, including friction and wear of both pin and disc. From these experiments and electron microscopy of the worn samples, the following conclusions can be drawn:

1) In the multi-step speed experiments, a hydrodynamic effect only affects friction and wear when using the 5 μm slurry as interfacial medium. No notable hydrodynamic effect can be observed for bigger particles (13 μm); because the large initial gap (13 μm) will make the speed-induced thickness variation negligible.

2) For multi-step speed experiments using the 5 μm slurry, a classical Stribeck curve-like behavior can be observed for friction as well as an increase in film thickness. The speed-induced hydrodynamic effect can extend the film thickness up to 14% and lead to a friction reduction of about 2/3.

3) An indent trajectory of distinct geometrical shapes appears on the worn surface at 400 mm/s, indicating that rolling of particles creates the indents.

4) For constant speed experiments using the 5 μm slurry and as a result of speed-induced hydrodynamic effect, a change from two-body abrasion to three-body abrasion and a change of the dominating wear mechanism from microcutting and microploughing to fatigue wear can be observed when the sliding speed increases from 50 to 400 mm/s.

5) A change in how the slurry particles move through the contact combined with a hydrodynamic effect at high speeds (400 mm/s) does not cause a reduction in the total amount of wear. However, the wear distribution between pin and disc changes significantly when the speed varies from 50 to 400 mm/s. These unexpected results are caused by the difference in friction power and dissipated power density in the tribological system.

Acknowledgements

We express our gratitude to the following funding agencies and collaborators: the European Research Council (ERC) under Grant No. 771237 (TriboKey), the China Scholarship Council (CSC) for awarding a scholarship to Yulong LI, and Nikolas SCHIFFMANN and Svenja DITTRICH for the assistance in the characterization of particles in the slurry.

Electronic Supplementary Material Supplementary material is available in the online version of this article at https://doi.org/10.1007/s40544-022-0654-1.

References

[1] Stolarski, T A. *Tribology in Machine Design*. Oxford (UK): Butterworth-Heinemann, 2000.

[2] Stachowiak G W, Batchelor A W. *Engineering Tribology*, 3rd edn. Amsterdam (The Netherlands): Butterworth-Heinemann, 2005.

[3] Zum Gahr K H. *Microstructure and Wear of Materials*. Amsterdam (The Netherlands): Elsevier Amsterdam, 1987.

[4] Misra A, Finnie I. A review of the abrasive wear of metals. *J Eng Mater Technol* **104**(2): 94–101 (1982)

[5] Czichos H. *Tribology: A Systems Approach to the Science and Technology of Friction, Lubrication and Wear*. Amsterdam (The Netherlands): Elsevier Science, 1978.

[6] Rabinowicz E, Dunn L A, Russell P G. A study of abrasive wear under three-body conditions. *Wear* **4**(5): 345–355 (1961)

[7] Misra A, Finnie I. A classification of three-body abrasive wear and design of a new tester. *Wear* **60**(1): 111–121 (1980)

[8] Zum Gahr K H. Wear by hard particles. *Tribol Int* **31**(10): 587–596 (1998)

[9] Sin H, Saka N, Suh N P. Abrasive wear mechanisms and the grit size effect. *Wear* **55**(1): 163–190 (1979)

[10] Misra A, Finnie I. Some observations on two-body abrasive wear. *Wear* **68**(1): 41–56 (1981)

[11] Misra A, Finnie I. Correlations between two-body and three-body abrasion and erosion of metals. *Wear* **68**(1): 33–39 (1981)

[12] Misra A, Finnie I. On the size effect in abrasive and erosive wear. *Wear* **65**(3): 359–373 (1981)

[13] Williams J A, Hyncica A M. Mechanisms of abrasive wear in lubricated contacts. *Wear* **152**(1): 57–74 (1992)

[14] Williams J A, Hyncica A M. Abrasive wear in lubricated contacts. *J Phys D: Appl Phys* **25**(1A): A81–A90 (1992)

[15] Tressia G, Penagos J J, Sinatora A. Effect of abrasive particle size on slurry abrasion resistance of austenitic and martensitic steels. *Wear* **376–377**: 63–69 (2017)

[16] Andrade M F C, Martinho R P, Silva F J G, Alexandre R J D, Baptista A P M. Influence of the abrasive particles size in the micro-abrasion wear tests of TiAlSiN thin coatings. *Wear* **267**(1–4): 12–18 (2009)

[17] Petrica M, Badisch E, Peinsitt T. Abrasive wear mechanisms and their relation to rock properties. *Wear* **308**(1–2): 86–94 (2013)

[18] Ren X Y, Peng Z J, Hu Y B, Rong H Y, Wang C B, Fu Z Q, Qi L H, Miao H Z. Three-body abrasion behavior of ultrafine WC–Co hardmetal RX8UF with carborundum, corundum and silica sands in water-based slurries. *Tribol Int* **80**: 179–190 (2014)

[19] Gee M G, Gant A, Hutchings I, Bethke R, Schiffman K, van Acker K, Poulat S, Gachon Y, von Stebut J. Progress towards standardisation of ball cratering. *Wear* **255**(1–6): 1–13 (2003)

[20] Petrica M, Katsich C, Badisch E, Kremsner F. Study of abrasive wear phenomena in dry and slurry 3-body conditions. *Tribol Int* **64**: 196–203 (2013)

[21] Yu R Z, Chen Y, Liu S X, Huang Z Q, Yang W, Wei W. Abrasive wear behavior of Nb-containing hypoeutectic Fe–Cr–C hardfacing alloy under the dry-sand/rubber-wheel system. *Mater Res Express* **6**(2): 026535 (2019)

[22] Xiao H P, Liu S H, Guo Y B, Wang D G, Chen Y. Effects of microscale particles as antiwear additives in water-based slurries with abrasives. *Tribol Trans* **59**(2): 323–329 (2016)

[23] Da Silva W M, Suarez M P, Machado A R, Costa H L. Effect of laser surface modification on the micro-abrasive wear resistance of coated cemented carbide tools. *Wear* **302**(1–2): 1230–1240 (2013)

[24] Vashishtha N, Sapate S G. Abrasive wear maps for High Velocity Oxy Fuel (HVOF) sprayed WC–12Co and Cr_3C_2–25NiCr coatings. *Tribol Int* **114**: 290–305 (2017)

[25] Kumar S, Balasubramanian V. Effect of reinforcement size and volume fraction on the abrasive wear behaviour of AA7075 Al/SiCp P/M composites—A statistical analysis. *Tribol Int* **43**(1–2): 414–422 (2010)

[26] Qi J W, Wang L P, Yan F Y, Xue Q J. The tribological performance of DLC-based coating under the solid–liquid lubrication system with sand-dust particles. *Wear* **297**(1–2): 972–985 (2013)

[27] Yakubov G E, Branfield T E, Bongaerts J H H, Stokes J R. Tribology of particle suspensions in rolling–sliding soft contacts. *Biotribology* **3**: 1–10 (2015)

[28] Richard Stribeck. *Die Wesentlichen Eigenschaften der Gleit- und Rollenlager*. Berlin (Germany): Springer Verlag, 1903. (in German)

[29] Kalin M, Velkavrh I, Vižintin J. The Stribeck curve and lubrication design for non-fully wetted surfaces. *Wear* **267**(5–8): 1232–1240 (2009)

[30] Spikes H A. Some challenges to tribology posed by energy efficient technology. In: Proceedings of the 24th Leeds-Lyon Symposium on Tribology, London, 1997.

[31] Braun D, Greiner C, Schneider J, Gumbsch P. Efficiency of laser surface texturing in the reduction of friction under mixed lubrication. *Tribol Int* **77**: 142–147 (2014)

[32] Greiner C, Schäfer M. Bio-inspired scale-like surface textures and their tribological properties. *Bioinspiration Biomim* **10**(4): 044001 (2015)

[33] Greiner C, Merz T, Braun D, Codrignani A, Magagnato F. Optimum dimple diameter for friction reduction with laser surface texturing: The effect of velocity gradient. *Surf Topogr Metrol Prop* **3**(4): 044001 (2015)

[34] Chen X, Schneider R, Gumbsch P, Greiner C. Microstructure evolution and deformation mechanisms during high rate and cryogenic sliding of copper. *Acta Mater* **161**: 138–149 (2018)

[35] Zum Gahr K H, Wahl R, Wauthier K. Experimental study of the effect of microtexturing on oil lubricated ceramic/steel friction pairs. *Wear* **267**(5–8): 1241–1251 (2009)

[36] Schneider J, Braun D, Greiner C. Laser textured surfaces for mixed lubrication: Influence of aspect ratio, textured area and dimple arrangement. *Lubricants* **5**(3): 32 (2017)

[37] Galda L, Pawlus P, Sep J. Dimples shape and distribution effect on characteristics of Stribeck curve. *Tribol Int* **42**(10): 1505–1512 (2009)

[38] Spikes H A. Mixed lubrication—an overview. *Lubr Sci* **9**(3): 221–253 (1997)

[39] Spikes H A, Olver A V. Basics of mixed lubrication. *Lubr Sci* **16**(1): 1–28 (2003)

[40] Liang H, Xu G H. Lubricating behavior in chemical–mechanical polishing of copper. *Scripta Mater* **46**(5): 343–347 (2002)

[41] Bahr M, Sampurno Y, Han R C, Philipossian A. Improvements in stribeck curves for copper and tungsten chemical mechanical planarization on soft pads. *ECS J Solid State Sci Technol* **6**(5): 290–295 (2017)

[42] Rovani A C, Rosso T A, Pintaude G. On the use of microscale abrasion test for determining the particle abrasivity. *J Test Eval* **49**(1): 20180576 (2021)

[43] Harsha A P, Tewari U S. Two-body and three-body abrasive wear behaviour of polyaryletherketone composites. *Polym Test* **22**(4): 403–418 (2003)

[44] Cozza R C, Tanaka D K, Souza R M. Friction coefficient and abrasive wear modes in ball-cratering tests conducted at constant normal force and constant pressure—Preliminary results. *Wear* **267**(1–4): 61–70 (2009)

[45] Spikes H A, Olver A V, Macpherson P B. Wear in rolling contacts. *Wear* **112**(2): 121–144 (1986)

[46] Wegener, K. Ploughing. In: *CIRP Encyclopedia of Production Engineering*. Luc L, Gunther R, Eds. Berlin (Germany): Springer Berlin Heidelberg, 2014: 1321–1327.

[47] Lawn B, Wilshaw R. Indentation fracture: Principles and applications. *J Mater Sci* **10**(6): 1049–1081 (1975)

[48] Cook R F, Pharr G M. Direct observation and analysis of indentation cracking in glasses and ceramics. *J Am Ceram Soc* **73**(4): 787–817 (1990)

[49] Sun G, Bhattacharya S, White D R, McClory B, Alpas A T. Indentation fracture behavior of low carbon steel thermal spray coatings: Role of dry sliding-induced tribolayer. *J Therm Spray Technol* **27**(8): 1602–1614 (2018)

[50] Cook R F. Fracture sequences during elastic–plastic indentation of brittle materials. *J Mater Res* **34**(10): 1633–1644 (2019)

[51] Blickensderfer R, Tylczak J H. A large-scale impact spalling test. *Wear* **84**(3): 361–373 (1983)

[52] Greiner C, Liu Z L, Schneider R, Pastewka L, Gumbsch P. The origin of surface microstructure evolution in sliding friction. *Scripta Mater* **153**: 63–67 (2018)

[53] Haug C, Ruebeling F, Kashiwar A, Gumbsch P, Kübel C, Greiner C. Early deformation mechanisms in the shear affected region underneath a copper sliding contact. *Nat Commun* **11**: 839 (2020)

[54] Dollmann A, Kauffmann A, Heilmaier M, Haug C, Greiner C. Microstructural changes in CoCrFeMnNi under mild tribological load. *J Mater Sci* **55**(26): 12353–12372 (2020)

[55] Greiner C, Liu Z L, Strassberger L, Gumbsch P. Sequence of stages in the microstructure evolution in copper under mild reciprocating tribological loading. *ACS Appl Mater Interfaces* **8**(24): 15809–15819 (2016)

[56] Landgraf R.W. *Cyclic Deformation and Fatigue Behavior of Hardened Steels*. Urbana (USA): Department of Theoretical and Applied Mechanics (UIUC), 1968.

[57] Bílý M. *Cyclic Deformation and Fatigue of Metals*. Amsterdam (the Netherlands): Elsevier Amsterdam, 1993.

[58] Sosnovskiy L A. *Tribo-Fatigue*. Berlin (Germany): Springer Berlin Heidelberg, 2005.

[59] Sciammarella C A, Chen R J S, Gallo P, Berto F, Lamberti L. Experimental evaluation of rolling contact fatigue in railroad wheels. *Int J Fatigue* **91**: 158–170 (2016)

[60] Brownlie F, Hodgkiess T, Galloway A M, Pearson A. Experimental investigation of engineering materials under repetitive impact with slurry conditions. *Tribol Lett* **69**(1): 5 (2021)

[61] Gates J D. Two-body and three-body abrasion: A critical discussion. *Wear* **214**(1): 139–146 (1998)

[62] Trezona R I, Allsopp D N, Hutchings I M. Transitions between two-body and three-body abrasive wear: Influence of test conditions in the microscale abrasive wear test. *Wear* **225–229**: 205–214 (1999)

[63] Torrance A A, d'Art J M. A study of lubricated abrasive wear. *Wear* **110**(1): 49–59 (1986)

[64] Ramalho A, Miranda J C. The relationship between wear

and dissipated energy in sliding systems. *Wear* **260**(4–5): 361–367 (2006)

[65] Dante R C, Vannucci F, Durando P, Galetto E, Kajdas C K. Relationship between wear of friction materials and dissipated power density. *Tribol Int* **42**(6): 958–963 (2009)

[66] Bose K, Wood R J K. Optimum tests conditions for attaining uniform rolling abrasion in ball cratering tests on hard coatings. *Wear* **258**(1–4): 322–332 (2005)

[67] Gomez V A O, de Macêdo M C S, Souza R M, Scandian C. Effect of abrasive particle size distribution on the wear rate and wear mode in micro-scale abrasive wear tests. *Wear* **328–329**: 563–568 (2015)

Yulong LI. He received his B.Sc. and M.Sc. degrees in metallurgy engineering from Northeastern University, China, focusing on material preparation and its tribology properties. Currently, he is a Ph.D. student in the Department of Mechanical Engineering at Karlsruhe Institute of Technology (KIT), Germany. His research interests range from abrasive wear to the influence of surface profile in tribology.

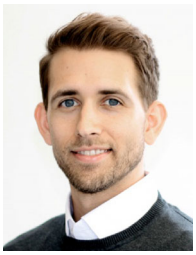

Paul SCHREIBER. He completed his master degree in mechanical engineering at the Karlsruhe Institute of Technology (KIT), Germany and subsequently earned his doctorate in the field of tribology in 2019. His research was focused mainly on the super-lubricious properties of ceramic materials and the influence of laser surface texturing on them. His postdoctoral time in the group of Christian GREINER at KIT mainly revolved around questions on the digitization of experimental tribology, in particular creating the pre-conditions for the generation of high-quality, interoperable measurement and metadata in accordance with the FAIR data principles.

Johannes SCHNEIDER. He received his diploma and Ph.D. degrees in mechanical engineering from the University of Karlsruhe, Germany, in 1992 and 1997 respectively. His current position is a Staff Scientist at the Institute for Applied Materials—Reliability and Microstructure (IAM—ZM) at the Karlsruhe Institute of Technology (KIT), Germany. His research interests include laser surface texturing and modification and its influence on friction and wear.

Christian GREINER. He obtained his master degree from the University of Stuttgart, Germany, in 2004 and his Ph.D. degree from the Max Planck Institute for Metals Research, Germany, in 2007. After a postdoc at the University of Pennsylvania, USA, he joined the Karlsruhe Institute of Technology (KIT), Germany, in 2010, where he became a full professor in 2021. He heads the Materials Tribology Group, mainly funded through a Consolidator Grant of the European Research Council (ERC). His research interests include microstructure property relations under a tribological load as well as bioinspired surface morphologies.